White-light symmetrization by the interaction of multifilamenting beams

K. Stelmaszczyk,[1] P. Rohwetter,[1] Y. Petit,[2] M. Fechner,[1] J. Kasparian,[2,*] J.-P. Wolf,[2] and L. Wöste[1]
[1]*Institut für Experimentalphysik, Freie Universität Berlin, Arnimallee 14, D14195 Berlin, Germany*
[2]*GAP-Biophotonics, Université de Genève, 20 rue de l'Ecole de Médecine, 1211 Geneva 4, Switzerland*
(Received 8 April 2009; published 29 May 2009)

We show experimentally that the interaction of two multifilamenting beams in fused silica with incidence angles up to a few degrees results in an increase in the symmetry of the continuum emission from D_2 to C_∞ around the axis of symmetry between the two beams. We observe an intense white disk between the locations of the individual conical emission patterns, reducing the conical emission in each of them. We attribute this behavior to an enhanced self-phase modulation in the interference region between the two beams. This frequency conversion depletes by more than 40% the energy initially available in the photon bath to feed filaments.

DOI: 10.1103/PhysRevA.79.053856 PACS number(s): 42.65.Jx, 42.65.Tg, 42.65.Ky

I. INTRODUCTION

Nonlinearity is known as capable to increase the symmetry of physical systems. This is, e.g., the case in the self-similar optical collapse, in which any incident beam profile submitted to Kerr self-focusing self-converts into a circular Townes profile [1].

Self-focusing can ultimately result in filamentation, which is due to a dynamic balance between the Kerr self-focusing and defocusing on the plasma generated at the nonlinear focus [2–6]. When the incident beam power largely exceeds the critical power P_{cr} of the propagation material ($P_{cr} \simeq 2.3$ MW in fused silica at 800 nm [7]), the beam profile breaks up into many cells, each one yielding one single filament. These filaments generated across the beam profile were shown to be coherent with one another, which allows them to interact. These interactions can take the form of repulsion or attraction of neighboring filaments [8–12] or interference of their conical emission [13]. Moreover, the interaction of the two incident laser photon baths can also lead to the attraction or repulsion of the resulting filaments of each individual beam, depending on their relative phase [14,15]. Adequate tuning of the relative incidence angle even allows the filaments from the two beams to merge into a central one [11], or to exchange energy, resulting in a partial extinction of the conical emission [16].

In this paper, we investigate the interaction of two multifilamenting beams in fused silica with incident angles up to a few degrees. We show that this interaction results in an increase in symmetry of the continuum emission from D_2 to C_∞ around the axis of symmetry between the two beams. An intense white disk is observed between the locations of the individual conical emission patterns, reducing or even almost suppressing the conical emission in each of them. We attribute this behavior to an enhanced self-phase modulation (SPM) in the interaction region, where the interference between the two beams redistributes the local wave vectors into a broad angular distribution. Frequency conversion depletes the energy initially available in the photon bath to feed filaments, similarly to the competition already observed in the case of a single beam [17].

The observed on-axis generation of the white light, while a significant fraction of the fundamental still propagates a few degrees apart, could be useful for spectroscopic applications to geometrically select the supercontinuum emission and reject this undeviated fraction of the fundamental wavelength.

II. EXPERIMENTAL SETUP

The experimental setup is depicted in Fig. 1. A femtosecond chirped-pulse amplification laser operating at $\lambda_0 = 800$ nm wavelength generates a train of pulses at a repetition rate of 10 Hz. The energy of each individual pulse is 20 mJ with a duration of 130 fs. The laser beam is divided in two parts by a thin 50:50% beam splitter. The most intense central part from each beam is selected by circular apertures of 2 mm diameter, letting, respectively, 1.2 and 1.3 mJ of energies to pass through. The beams then interact inside a 20-mm-thick fused silica block. The optimal temporal overlap is adjusted by translating a bending mirror in one arm. Visual observation as well as true-color imaging from the top of the fused silica block showed the occurrence of multiple filamentation when the two beam propagate independently as well as when they overlap temporally.

The interaction between the beams was investigated at four incidence angles $2\theta_0' = 3.0°$, 3.2°, 3.8°, and 4.5° (full angles) in air, corresponding to $2\theta_0 = 2.1°$, 2.2°, 2.6°, and 3.1° in the fused silica block, respectively. The far-field pat-

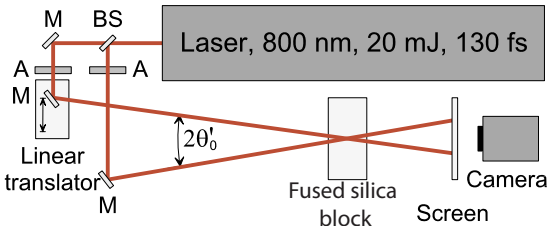

FIG. 1. (Color online) Experimental setup: BS: beam splitter, A: circular aperture, and M: mirror.

*jerome.kasparian@unige.ch

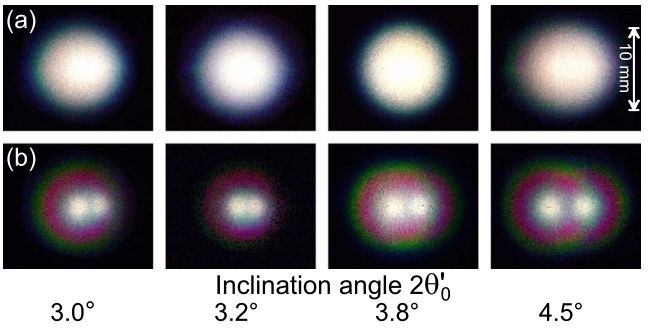

FIG. 2. (Color online) Far-field beam image on a screen at a distance of 40 mm from the fused silica block as a function of the angle between the incident beams (a) with and (b) without temporal overlap between the pulses.

tern of the white-light emission was recorded with a color-frame digital camera, on a diffusing screen placed 40 mm behind the substrate. Besides, the spectrum of the emitted continuum was analyzed using a miniature spectrometer, with 0.34 nm resolution. In order to record the full dynamics of the spectrum, which spans over more than 4 orders of magnitude, different neutral density filters were used for different spectral ranges, which were then cross normalized to reconstruct the full spectra. The emitted light was collected by a Teflon integrating sphere. The angular distribution of the white-light spectrum was recorded by horizontally translating the sphere across the plane defined by the two incident beams, at a distance of 275 mm from the fused silica block. In this configuration, the 5 mm input port of the integrating sphere provided an angular resolution of 1°.

III. EXPERIMENTAL RESULTS

Figure 2 displays such far-field image. Without interaction, each beam propagates independently and yields a small ($\lesssim 3-4$ nm) white spot with the corresponding conical emission [see also Figs. 3(a) and 3(c)]. In contrast, the interaction of the two pulses yields remarkably strong white light and a much broader (~ 10 nm) circular spot encompassing the positions of both beams [Fig. 3(b)]. In addition, the conical emission disappears. The white color of the spot as well as its size and shape are very similar for all investigated incidence angles. At larger incidences the efficiency of the white-light emission is noticeably lower and the transition from a circular to elliptical spot profile is observed. This tendency is already visible in Fig. 2(a) for $2\theta_0'=4.5°$.

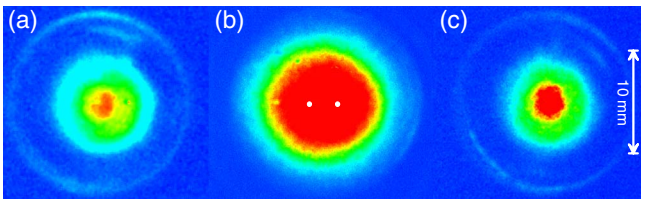

FIG. 3. (Color online) Intensity distribution of the white-light generation at 436 nm, for an incidence angle of $2\theta_0'=3.5°$. (a) Noninteracting left beam, (b) two interacting beams, and (c) noninteracting right beam. The intensity scale is normalized independently for each of the image. Reduction in conical emission is clearly visible for interacting beams (b), where the two white dots indicate the positions of individual beams respective to the white-light spot.

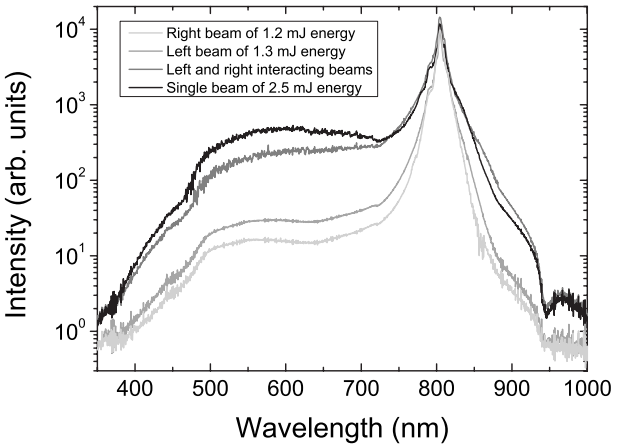

FIG. 4. Influence of the two-beam interaction on the white-light spectrum. The spectra are assembled from several spectrum sections recorded with different optical density filters and normalized to each other.

The generation of a bright white spot qualitatively observed on the screen, as mentioned above, indeed corresponds to a tenfold increase in the supercontinuum generation in the 450–700 nm region, as well as around 900 nm, as compared with the individually propagating beams (Fig. 4). This spectral broadening is practically independent from the incidence angle over the whole investigated interval of incident angles. The two interacting beams generate white-light continuum almost as efficiently as one single beam that would bear their whole energy, depleting the fundamental wavelength by more than 40%.

Both with and without interactions between the beams, the angular distribution of the white-light spectrum (Fig. 5) is dominated by the peak at the fundamental wavelength around $\pm 1.6°$, i.e., at the original location of each incident beam. However, the interaction results in a reduction in the fundamental emission at 0° and a transversely more homogeneous spectrum, between −3° and +3°. This homogeneity corresponds to the visual observation of an homogeneous white spot on a screen in the far field. Also, the conical emission [dotted line on panel (a)] disappears almost completely when the two beams overlap temporally.

IV. DISCUSSION

The observed generation of a white-light disk in the forward direction may at once remind us of the interaction [14,15] or even the merging [11] of the filaments from two crossing beams. However, such merging occurs at very small incident angles, typically 20–30 times smaller than in our experiment [11]. Moreover, we observed neither evidence of filament merging into new filaments oriented along the z axis on photographs taken from the top of the fused silica block nor conical emission, i.e., concentric colorful rings coaxial with the forward-emitted white light. We therefore conclude

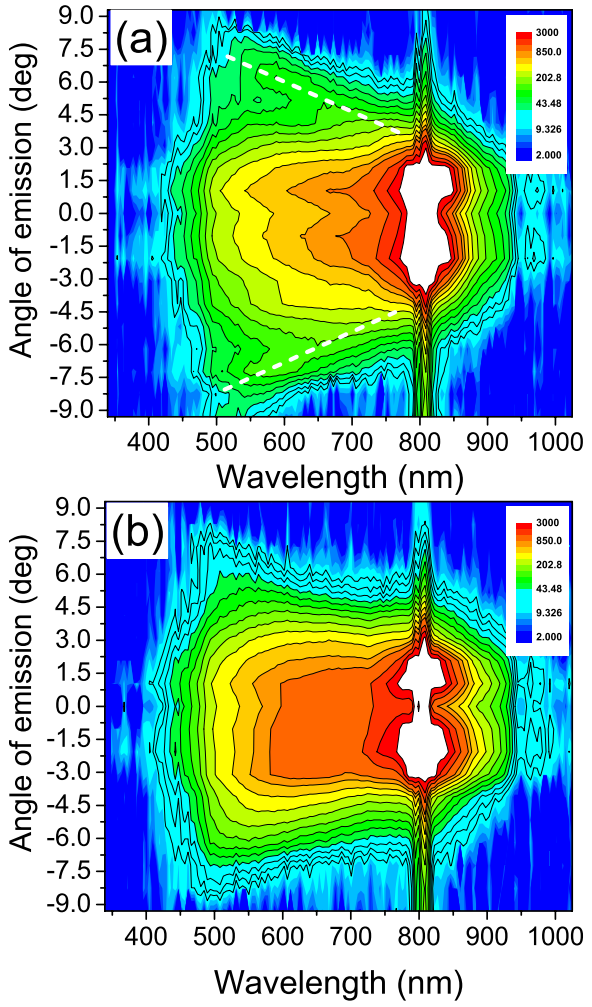

FIG. 5. (Color online) Angular distribution of the white-light spectrum for (a) noninteracting and (b) interacting beams with an incident angle of $2\theta_0'=3.2°$ ($2\theta_0=2.2°$). Both graphs share the same logarithmic scale in intensity. Note that the interaction results in (i) a strong reduction in the conical emission [dotted lines in panel (a)], (ii) the generation of an homogeneous spectrum between $-1.5°$ and $1.5°$, as shown by the wide flat region of panel (b), and (iii) a reduced fundamental intensity at $0°$, as shown by a narrowing of the white (saturated) region of panel (b).

that the process at play does not specifically depend on the occurrence of filamentation.

Instead, we interpret our observations based on a partial inhibition of filamentation due to a more efficient white-light continuum generation in the photon bath where the two beams interact through SPM and cross-phase modulation (XPM). The observed efficient depletion of the fundamental wavelength by the white-light generation reduces its power available to feed the filaments. This results in a less efficient filamentation and hence in a sharp decrease in the brightness of the associated conical emission at the exit of the fused silica block.

In the interaction region, the interference between the two beams redistributes the directions of the wave vectors, thus loosing the initial D_2 symmetry defined by the two incident beams. Instead, the wide range of wave-vector directions results in a revolution (C_∞) symmetry around the z axis, independently of the incidence angle. Moreover, due to the relatively large incidence angle, no interference pattern can be resolved in the far field. This is consistent with the report by Corsi *et al.*, who reported such interference with a narrower incidence angle and observed that the white-light fringes tend to merge when the angle increases above $0.5°$ [18].

The interference between the two beams does not only impact the spatial symmetry of the supercontinuum emission, but also its intensity, locally doubling the incident electric field, i.e., quadrupling the incident intensity. Note that the transient grating [19] originating from the interference pattern has a typical step of $\lambda_0/2\sin(\theta_0)\sim 15\ \mu\mathrm{m}\gg\lambda_0$, yielding a typical width of $2\theta_0\sim 3°$ for the zero-order spot, so that no fringes are visible within the spot on the screen. On the other hand, illuminating a glass block with a cylindrical lens also resulted in a similar circular spot, although the incident angles θ_0 continuously range from $-5°$ to $5°$, thus blurring any interference pattern. We can therefore exclude diffraction on this interference pattern as the origin of the observed circular white spot.

The above discussion in terms of SPM can easily be transposed in terms of four-wave mixing (FWM), since both formalisms and SPM provide equivalent descriptions of the same physical processes if the wavelengths are quasidegenerate and the main active process is the conversion of the central wavelength into the supercontinuum. In a first step, we shall address the change in symmetry from D_2 to C_∞. In FWM, two photons at λ_1 and λ_2 mix up to generate two photons at λ_3 and λ_4. In this process, the energy conservation imposes $\omega_1+\omega_2=\omega_3+\omega_4$ (ω_i being the frequency associated with λ_i), while the phase matching condition sets $\vec{k_1}+\vec{k_2}=\vec{k_3}+\vec{k_4}$, where $k_i=2\pi n_i/\lambda_i$. As a consequence the plane defined by $\vec{k_3}$ and $\vec{k_4}$ can spin around $\vec{k_1}+\vec{k_2}$, adding one degree of freedom to the system. If the wavelengths of the incident photons lie within the spectral peak of the incident fundamental pulse, $k_1\sim k_2\sim k_0$, the direction of $\vec{k_1}+\vec{k_2}$ is close to the z axis. This degree of freedom is characterized by the angle ϕ_3 between the planes, respectively, defined by $(\vec{k}_1,\vec{k}_2)$ and $(\vec{k}_3,\vec{k}_4)$ and results in a circular (C_∞) symmetry of the emission.

However, such circular symmetry in a process driven by phase matching would at first be expected to generate colored rings rather than a white circular spot. Such spot can be understood if we consider quasidegenerate FWM events, i.e., with all λ_i close to λ_0. Such events have a very high occurrence probability due to an efficient pumping and seeding by the fundamental wavelength itself and intrinsic phase matching. However, their net impact on the pulse spectrum is negligible because many events of opposite directions statistically compensate each other. As a consequence, quasidegenerate FWM events are not considered in usual conditions. In our configuration with crossing beams, however, spectrally quasidegenerate events must be considered because they result in the emission of photons within the incident fundamental spectral peak, but in directions outside those of the initial beams so that it yields a net geometrical effect. More specifically, the output photons at wavelengths λ_3 and λ_4 are emitted at angles

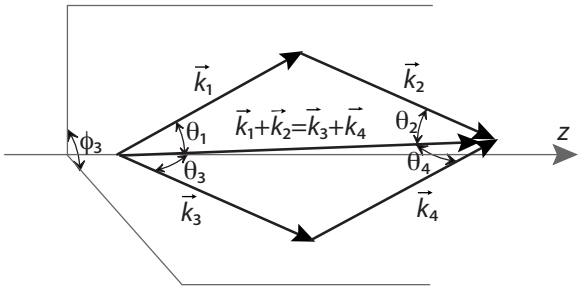

FIG. 6. Definition of the geometry of the proposed interpretation in terms of FWM

$$\theta_3 = \arccos\left(\frac{k_3^2 - k_4^2 + (k_1+k_2)^2\cos^2\theta_0}{2k_3(k_1+k_2)\cos\theta_0}\right), \quad (1)$$

$$\theta_4 = \arccos\left(\frac{k_4^2 - k_3^2 + (k_1+k_2)^2\cos^2\theta_0}{2k_4(k_1+k_2)\cos\theta_0}\right), \quad (2)$$

as derived from the cosine theorem in the triangle formed by $\vec{k_1}+\vec{k_2} \simeq (k_1+k_2)\cos\theta_0\vec{u_z}$, $\vec{k_3}$, and $\vec{k_4}$ (Fig. 6). θ_3 and θ_4 obviously depend on λ_1 and λ_2, so that the spectral width of the incident pulses provides a supplementary spatial degree of freedom. Scanning those wavelengths across the input spectrum therefore yields the angular distribution of the emission of λ_3 and λ_4. Furthermore, since FWM events are cascading, Eqs. (1) and (2) will iteratively increase the two-dimensional divergence of the fundamental wavelength, in a process similar to that recently described by Majus *et al.* [20].

We simulated such geometric broadening of the incident peaks for up to 50 cascaded FWM events. In each step, λ_1 and λ_2 are scanned from 775 to 825 nm, and generation of photons at λ_3 set to $\lambda_3 = 2\lambda_0 - \lambda_1$ is considered, with $\lambda_0 = 800$ nm. The generation efficiency is assumed to be proportional to the intensity of λ_1 and λ_2 in the initial spectrum. The same processing is iterated, assuming that the spectrum is unaffected by the considered processes, by bootstrapping θ_3 as the input θ_0 for the next iteration. As displayed in Fig. 7, the fundamental radiation spreads over a wide angular range. The photon bath in the initial direction of the beams, available to sustain filamentation within those beams, is clearly depleted, while the two beams merge into a more homogeneous angular distribution of the fundamental wavelength, which bridges the gap between the two beams after typically 40 iterations.

It should be noted that, in this simple calculation, only the efficiently seeded in-plane FWM events have been taken into account. However, the emission can occur in any plane around the z axis. As a consequence, a supplementary degree of freedom should be considered, yielding an even faster and more efficient spatial broadening. Moreover, our simulation is restricted to the fundamental wavelength of the incident beams due to computing limitations, but it could in principle be extended to the full spectrum of the white-light continuum. It would then obviously yield a similar angular spreading of the beam, resulting in the bright white spot observed in the experiments.

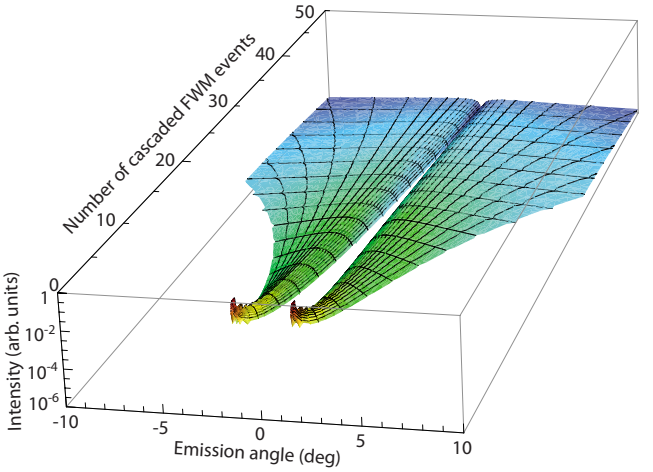

FIG. 7. (Color online) Angular broadening of the incident pulses. The plot displays the calculated intensity integrated over the 775–825 nm range as a function of the angle, for up to 50 cascaded FWM events (see text for details).

V. CONCLUSION

In conclusion, we have shown that two ultrashort beams crossing at an angle of a few degrees in fused silica with adequate relative delay result in a qualitative change in the emission pattern of the continuum. While this pattern is composed of two sets of conical emission rings when the two beams propagate independently, their interaction results in a bright white circular spot, encompassing the directions of the two incident beams. This pattern change is the signature of SPM within the field resulting from the interference of the two incident beams. Moreover, the spectral broadening of the photon bath competes with the feeding of filamentation, largely reducing its contribution to the final far-field pattern.

The difference in the emission geometry of the white-light continuum and of the fundamental wavelength allows us to geometrically select the supercontinuum for spectroscopic applications of the white-light supercontinuum, such as remote sensing [3,21] or supercontinuum cavity ring-down spectroscopy [22]. For example, in our experimental arrangement, the overall losses in the blue green (BG) part of the spectrum can be less than 20–30 %, while a 2-mm-thick BG colored glass filter would reject 50–60 % of the light in the same spectral region.

ACKNOWLEDGMENTS

This work was supported by the Swiss NSF (Contracts No. 200021-111688 and No. 200021-116198 and R'equip program). We greatly acknowledge fruitful discussions with Dr. Bruno Schmidt about the arrangement of the experimental setup.

[1] K. D. Moll, A. L. Gaeta, and G. Fibich, Phys. Rev. Lett. **90**, 203902 (2003).
[2] A. Braun, G. Korn, X. Liu, D. Du, J. Squier, and G. Mourou, Opt. Lett. **20**, 73 (1995).
[3] J. Kasparian and J.-P. Wolf, Opt. Express **16**, 466 (2008).
[4] L. Bergé, S. Skupin, R. Nuter, J. Kasparian, and J.-P. Wolf, Rep. Prog. Phys. **70**, 1633 (2007).
[5] A. Couairon and A. Mysyrowicz, Phys. Rep. **441**, 47 (2007).
[6] S. L. Chin, S. A. Hosseini, W. Liu, Q. Luo, F. Theberge, N. Akozbek, A. Becker, V. P. Kandidov, O. G. Kosareva, and H. Schroeder, Can. J. Phys. **83**, 863 (2005).
[7] S. Tzortzakis, L. Sudrie, M. Franco, B. Prade, A. Mysyrowicz, A. Couairon, and L. Bergé, Phys. Rev. Lett. **87**, 213902 (2001).
[8] L. Bergé, M. R. Schmidt, J. J. Rasmussen, P. L. Christiansen, and K. Ø. Rasmussen, J. Opt. Soc. Am. B **14**, 2550 (1997).
[9] C. Ren, R. G. Hemker, R. A. Fonseca, B. J. Duda, and W. B. Mori, Phys. Rev. Lett. **85**, 2124 (2000).
[10] S. A. Hosseini, Q. Luo, B. Ferland, W. Liu, S. L. Chin, O. G. Kosareva, N. A. Panov, N. Aközbek, and V. P. Kandidov, Phys. Rev. A **70**, 033802 (2004).
[11] T.-T. Xi, X. Lu, and J. Zhang, Phys. Rev. Lett. **96**, 025003 (2006).
[12] Ma Yuan-Yuan, Lu Xin, Xi Ting-Ting, Hao Zuo-Qiang, Gong Qi-Huang, and Zhang Jie, Chin. Phys. **16**, 2731 (2007).
[13] S. L. Chin, S. Petit, W. Liu, A. Iwasaki, M. C. Nadeau, V. P. Kandidov, O. G. Kosareva, and K. Y. Andrianov, Opt. Commun. **210**, 329 (2002).
[14] A. A. Ishaaya, T. D. Grow, S. Ghosh, L. T. Vuong, and A. L. Gaeta, Phys. Rev. A **75**, 023813 (2007).
[15] Y. Y. Ma, X. Lu, T. T. Xi, Q. H. Gong, and J. Zhang, Appl. Phys. B: Lasers Opt. **93**, 463 (2008).
[16] A. C. Bernstein, M. Mc Cormick, G. M. Dyer, J. C. Sanders, and T. Ditmire, Phys. Rev. Lett. **102**, 123902 (2009).
[17] D. Faccio, A. Averchi, A. Couairon, A. Dubietis, R. Piskarskas, A. Matijosius, F. Bragheri, M. A. Porras, A. Piskarskas, and P. Di Trapani, Phys. Rev. E **74**, 047603 (2006).
[18] C. Corsi, A. Tortora, and M. Bellini, Appl. Phys. B: Lasers Opt. **78**, 299 (2004).
[19] H. J. Eichler, P. Gunter, and D. W. Pohl, *Laser-Induced Dynamic Gratings* (Springer, Berlin, 1986).
[20] D. Majus, V. Jukna, G. Valiulis, and A. Dubietis, Phys. Rev. A **79**, 033843 (2009).
[21] J. Kasparian, M. Rodriguez, G. Méjean, J. Yu, E. Salmon, H. Wille, R. Bourayou, S. Frey, Y.-B. André, A. Mysyrowicz, R. Sauerbrey, J.-P. Wolf, and L. Wöste, Science **301**, 61 (2003).
[22] K. Stelmaszczyk, P. Rohwetter, M. Fechner, M. Queiβer, A. Czyżewski, T. Stacewicz, and L. Wöste, Opt. Express **17**, 3673 (2009).